

# $\delta^{13}C$ , $CO_2/{}^3He$ and ${}^3He/{}^4He$ ratios reveal the presence of mantle gas in the $CO_2$ -rich groundwaters of the Ardenne massif (Spa, Belgium)

Agathe Defourny<sup>1,2</sup>, Pierre-Henri Blard<sup>3,4</sup>, Laurent Zimmermann<sup>3</sup>, Patrick Jobé<sup>2</sup>, Arnaud Collignon<sup>2</sup>, Frédéric Nguyen<sup>1</sup>, and Alain Dassargues<sup>1</sup>

<sup>1</sup>Urban and Environmental Engineering, University of Liège, Belgium

<sup>2</sup>Water Resource Departement, Spadel S.A., Belgium

<sup>3</sup>CRPG, Université de Lorraine, CNRS, UMR7358, Nancy, France

<sup>4</sup>Laboratoire de Glaciologie, ULB, Brussels, Belgium

**Correspondence:** Agathe Defourny (adefourny@uliege.be)

**Abstract.** Although natural  $CO_2$ -rich groundwaters of eastern Belgium have been known for centuries, the exact origin of their gas is still unclear. This paper presents the results of a sampling campaign in the area (Spa, Stoumont, Malmedy): 30 samples of both carbogaseous and non-carbogaseous groundwaters were analyzed for major elements,  $CO_2$  content and carbon isotopic composition. Among them, 13 samples were also analyzed for  ${}^3He/{}^4He$  and  ${}^4He/{}^{20}Ne$  ratios. The combination of  $\delta^{13}C$  (between ca.  $-9\text{‰}$ VPDB and  $-2\text{‰}$ VPDB),  $CO_2/{}^3He$  ratio (between  $1.9 \times 10^8$  and  $2.9 \times 10^9$ ) and  ${}^3He/{}^4He$  (between 0.92 and 2.70 Ra) shows with a high level of confidence that the  $CO_2$  in the carbogaseous groundwater of Spa and Bru has a mantle origin. It can likely be attributed to the degassing of mantle from the neighboring Eifel Volcanic Fields, located at a distance of 100 km eastwards.

The identity and nature of the deep-rooted fractures that act as  $CO_2$  transport pathway to the surface are still to be clarified, but several major thrust faults exist in the Rhenish Massif and could connect the Eifel Volcanic Field with the studied area.

## 1 Introduction

$CO_2$ -rich groundwaters have always been a very fascinating geomanifestation and their presence in a region is often the trigger of a strong economic and touristic activity. Lately, a better assessment of  $CO_2$  circulation modes in the sub-surface has gained in interest, as it is important to finely document their contribution to the natural budget of atmospheric  $CO_2$ . Understanding the saturation state of  $CO_2$  in groundwaters and in geological reservoirs is also important for  $CO_2$  storage projects. Moreover, in areas where  $CO_2$ -rich groundwater is bottled as mineral water, it is essential to have a complete understanding of the whole system, to ensure sustainable exploitation of the resource. The presence of  $CO_2$  in groundwater - in excess compared to the atmospheric equilibrium - can result from different phenomena, the most common ones being a direct contribution from the mantle, the dissolution of carbonate rocks, or an organic origin (Agnew 2018). The discharge of  $CO_2$  from deep geological structures to the surface is always the result of a specific geological context which involves a source of  $CO_2$  at depth and an intricate system of faults acting as transport pathways to the local groundwaters, considered as the final receptor.

This study focuses on the dozen of CO<sub>2</sub>-rich groundwater springs that exist in the Ardenne Massif, in Eastern Belgium. The most famous ones are located in the small city of Spa, whose springs have been known since the Roman Empire. The name of the town became famous thanks to the development of thermalism in the 19th century and is now used worldwide to refer to wellness and bathing activities. These groundwaters yield natural springs at the surface, but they are also exploited as mineral water from boreholes. Their CO<sub>2</sub> content ( $2 \pm 0.5$  g/l) makes them slightly acidic (pH around 5.7). They have a high content in iron ( $17 \pm 10$  mg/l on average, but up to 50 mg/l). They however bear a relatively low TDS (Total Dissolved Solid) with a dry residue ranging between 80 mg/l and 160 mg/l in comparison with other naturally sparkling mineral waters bottled in other European geological contexts (e.g., 940 mg/l for San Pellegrino, 1100 mg/l for Badoit, 3325 mg/l for Vichy Celestins, as stated on bottle labels).

Although these springs have been bottled for centuries and studied for many years, the origin of their high CO<sub>2</sub> content has not been established already. Helium isotopes, elemental <sup>4</sup>He/<sup>20</sup>Ne and CO<sub>2</sub> isotopic composition of dissolved gas are powerful tools to identify the sources of these gas (Sano and Marty 1995; Karolyte et al. 2019; Gilfillan et al. 2019). In this paper, we present the <sup>3</sup>He, <sup>4</sup>He, <sup>20</sup>Ne and CO<sub>2</sub> concentrations measured in 13 groundwater samples of the Spa and Bru areas (Ardennes, Belgium), together with hydrochemical analysis on major elements for 30 samples, to identify the origin of dissolved CO<sub>2</sub> in groundwater and to explore the potential hydro-connection with the Eifel Volcanic Fields (Western Germany), where similar CO<sub>2</sub> rich groundwaters are found.

## 2 Geological context

### 2.1 Regional geology

CO<sub>2</sub>-rich mineral waters from eastern Belgium are located in the Rhenish Massif, which is part of the Rhenohercynian fold belt (Vanbrabant, Braun, and Jongmans 2002). This massif extends through western Germany, eastern Belgium, Luxembourg, and a part of France, as shown in Figure 1. The Rhenish Massif is dominated by Paleozoic rocks and is separated into two parts by the Rhine Graben. The Western part, the Ardennes (eastern Belgium), is bordered in the north by the Midi-Eifel thrust fault. In the Ardennes region, the Rhenish Massif is dominated by the Ardenne Allochtone, consisting of a Cambro-Ordovician basement unconformably overlain by Devono-Carboniferous sandstones and limestones (Barros et al. 2021) (Figure 1).

The present regional geology is the result of several stages. The oldest rocks that can be observed in Belgium are found in the Ardennes region, they consist in Cambrian to Ordovician sediments deposited in deep platform marine environments. They mainly consist of fine clays in alternation with sandstones. During the Late Silurian, the Caledonian orogeny faulted and folded these layers and induced a strong metamorphism. Compression and shearing of claystone produced a well-expressed schistosity, while sandstone evolves into quartzites. The metasediments observed today are therefore an alternation of clays and sandstones metamorphosed into slates ("phyllades") and quartzites, which are called "quartzophyllades" in the region. Then, after an emersion and erosion period, sedimentary deposition started again during the Lower Devonian, in unconformity over

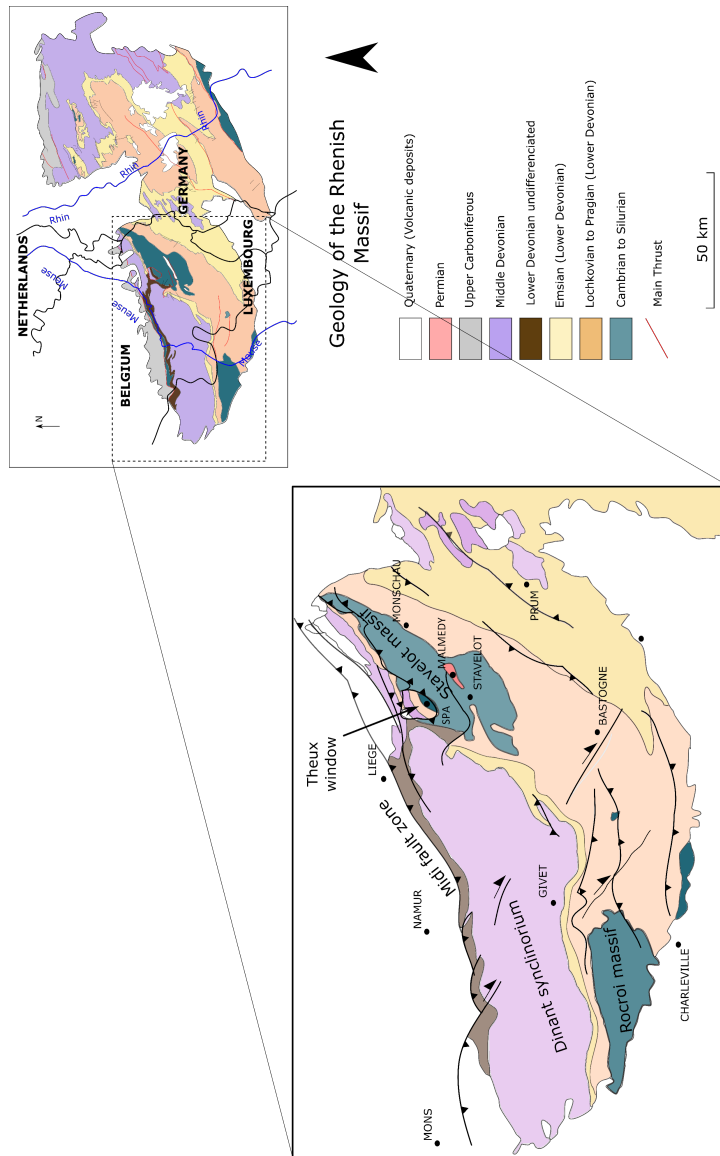


**Figure 1.** Simplified geology of the Ardennes Allochthon and its localisation in western Europe and in the Rhenish Massif, modified after Fielitz and Mansy 1999.

the folded rocks. During the Lower Devonian period, limestones were deposited in vast carbonate platforms. Then, sandstones accumulated in coastal detrital environments during the Devonian.

At the end of the Devonian, the Variscan orogeny took place, inducing another phase of tectonic deformation. During this orogeny, the Synclinorium of Dinant and the Ardenne Massif were displaced several kilometers northward. This (latter) unit constitutes the Ardennes Allochthone, a great anticlinal ensemble that is limited to the north by the Midi-Eifel thrust fault.

Three Cambrian massifs are identified within the Ardenne Allochtone: the Rocroi, the Givonne and the Stavelot massifs. The studied springs are located within the Stavelot Massif and at its border with the Dinant Synclinorium. The Graben of Malmedy, filled with Permian conglomerates, developed in the center of the Stavelot Massif with an SW-NE orientation is separating the Stavelot Massif into two parts (Barros et al. 2021).

## 2.2 CO<sub>2</sub>-rich groundwater springs in the Rhenish Massif and the Eifel volcanic fields

Numerous occurrences of CO<sub>2</sub>-rich groundwater springs are recorded in the Rhenish Massif, as shown in Figure 2. CO<sub>2</sub>-rich groundwaters present in Belgium are cold waters (12 °C on average). They are fed by the recharge from local or regional precipitations, as confirmed by <sup>18</sup>O and <sup>2</sup>H isotopic measurements (Barros et al. 2021). The system is dominated by metamorphosed sedimentary rocks and the aquifer zones lie in the first hundreds of meters of these deposits, in the fractured and weathered parts.

Naturally sparkling groundwaters are bottled by three different companies in the area (Bru-Chevron and Spa Monopole in Belgium, and Gerolsteiner Brunnen in Germany). While it has been proven several years ago that the dissolved CO<sub>2</sub> present in the springs of western Germany was the result of mantle degassing, this was not confirmed for the Belgian springs yet (May, Hoernes, and Neugebauer 1996; Aeschbach-Hertig et al. 1996; Barros et al. 2021).

However, the proximity between the two gas-rich groundwater areas, their common geological context, and the scale of the Eifel volcanism suggests that the gas they contain might have a common origin. In the Eifel area, volcanic activity has occurred during the Quaternary. It is thought that the lower mantle upwelling under central Europe may feed smaller upper-mantle plumes (Goes, Spakman, and Bijwaard 1999). Indeed, small plume structures have been identified below the Eifel area by teleseismic tomography (see Ritter et al. 2001) and a recent study by Kreemer et al. (2020) has shown that this plume was still buoyant (Kreemer, Blewitt, and Davis 2020). However, recent studies on the isotopic composition of noble gaz in the Eifel area and in Massif Central (France), tend to confirm a direct contribution from the upper mantle (MORB). The exact origin of the Eifel volcanism is thus still a matter of debate (Bekaert et al. 2019; Moreira et al. 2018).

## 3 Sampling and analysis

For this study, water samples from both natural springs and wells were collected at 30 different locations distributed within an area of (30 km x 20 km), belonging either to Spa, Bru or Malmedy regions (Table 1, Figure 3). Each of them has been analyzed for major and trace elements, physicochemical parameters, dissolved gases (O<sub>2</sub>, CO<sub>2</sub>, He, Ne) and carbon isotopes ( $\delta^{13}C$ ). During a second campaign, 13 of these 30 sites were resampled, with the specific purpose of analyzing their <sup>3</sup>He/<sup>4</sup>He and <sup>4</sup>He/<sup>20</sup>Ne isotopic ratios. Samples were stored into copper tubes clamped on both sides to prevent any degassing or air

## Volcanic activity and CO<sub>2</sub>-rich groundwater springs in the Rhenish Massif

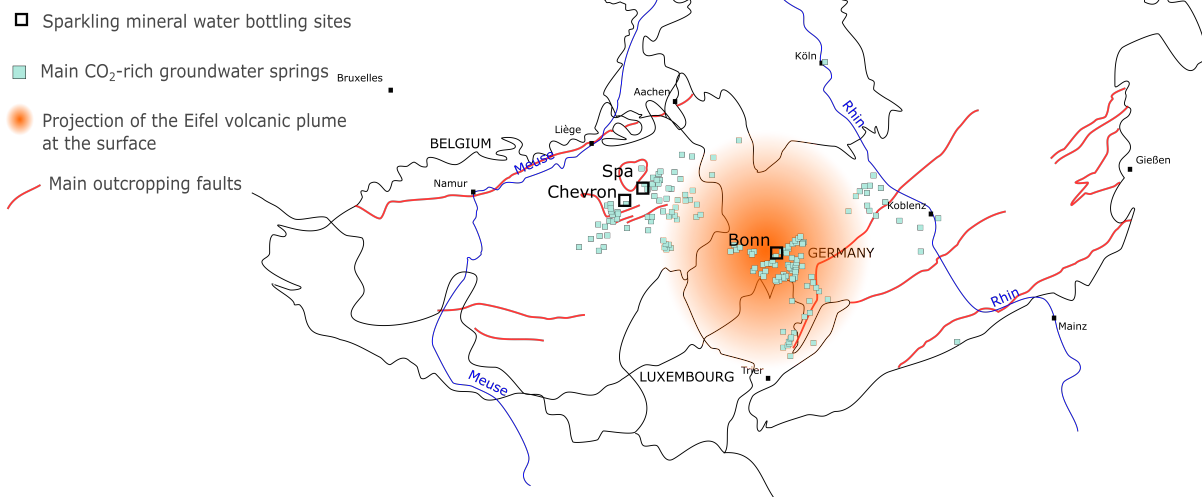


**Figure 2.** Occurrences of CO<sub>2</sub>-rich groundwater springs in the Rhenish Massif, together with the main bottling sites. The springs locations were compiled from May, Hoernes, and Neugebauer 1996; Bräur et al. 2013 and intern data from Spadel. The projection of the Eifel volcanic area is depicted after Bräur et al. 2013.

contamination.

95

Major and **trace** elements, together with physicochemical parameters and dissolved O<sub>2</sub> and CO<sub>2</sub>, were measured at the Spadel hydrochemistry laboratory, following the specific certified procedures: ISO 10523 (pH), ISO 7888 (electrical conductivity), ISO 10304-1 (chlorides, sulfates, and nitrates), ISO 9963 (bicarbonates), ISO 17289 (dissolved oxygen) and ISO 17294 (ICP-MS for the rest of the elements). Dissolved CO<sub>2</sub> was quantified by mineral sequestration via a barium sulfate saturated solution, followed by an inverse titration. Carbon isotopic ratios were measured by a private lab using isotope-ratio mass spectrometry (IRMS) and gas-chromatography isotope-ratio mass-spectrometry (GC-IRMS). Finally, the dissolved concentrations of helium isotopes were analyzed at the CRPG of Nancy (CNRS-UMR 7358) by static vacuum mass spectrometry after vacuum extraction and purification according to **Zimmermann and Bekaert (2020) and Zimmermann et al. (2015)**. <sup>4</sup>He/<sup>20</sup>Ne ratio was also measured in the same water aliquots, with a quadrupole installed on the extraction line. Instrument sensitivity was determined against a gas standard having an atmospheric composition. Tap water that had been placed in equilibrium with the atmosphere was also analyzed for comparison (Table 1).

105

Figure 3 shows the location of each sample in the local geology.

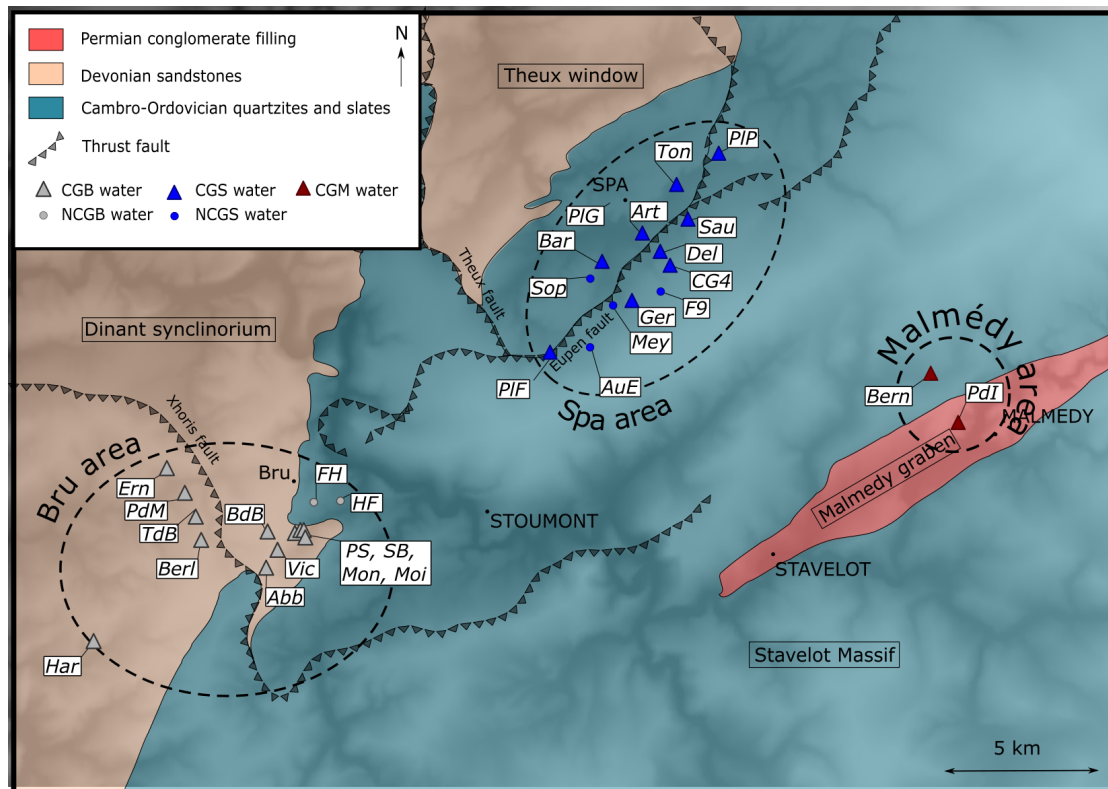


**Figure 3.** Location of each sample in regard with the main geological features.

## 4 Results

110 Table 1 presents the gas results measured in our 30 new samples. Data from Victoriaquelle (VQ) and Schwefelquelle (SQ) are from [Marty et al. \(2020\)](#). Data from the Laacher See Mofetta (LaS) and Wehr 10 well (W10) (Bräuer et al. 2013) are also included (i.e., a mofetta is a fumarole discharging mostly carbon dioxide). All these values can be compared to the Mid-ocean ridge basalts (MORB) endmember, which is commonly accepted to represent the signature of the upper mantle and have been studied in detail by [Graham \(2002\)](#).

115

Type	pH	CE $\mu S/cm$	Ca mg/l	Mg mg/l	Na mg/l	K mg/l	Cl mg/l	SiO <sub>2</sub> mg/l	HCO <sub>3</sub> mg/l	SO <sub>4</sub> mg/l	Fe mg/l	Mn mg/l	CO <sub>2</sub> g/l	O <sub>2</sub> mg/l	$\delta^{13}C$ DIC $\pm 0.3$ ‰ ‰VPDB	R/Ra	<sup>4</sup> He/ <sup>20</sup> Ne $\pm$		
BdB	5.2	301	21	15.63	6.92	1.67	3.3	20.84	143	<5	16.19	1.39	2.68	2.47	-2.4	2.7	0.02	150.63	9.55
Moi	5.4	424	25.7	24.93	8.51	1.71	4.2	17.58	234	<5	25.15	1.86	1.81	2.89	-2.9				
Mon	5.6	556	68.4	23.24	13.1	1.75	5	21.24	315	<5	7.05	1.3	2.02	2.86	-3.4	2.42	0.02	154.35	5.4
SB	5.1	232	12.3	11.43	7.46	0.97	3.9	20.98	91	<5	13.93	1.14	2.15	3.58	-3.4				
Abb	5.9	274	23.4	12.91	8.7	0.78	4	30.9	152	7.5	6.77	1.36	0.7	9.49	-8.8	2.61	0.02	68.16	2.7
PdM	5.9	223	23.9	10.76	5.65	1.07	12.8	7.07	100	<5	7.46	0.48	0.77	6.95	-8.7	2.42	0.01	33.19	1.54
PS	5.3	454	23.7	24.1	4.67	1.5	3.4	17.7	231	<5	35	2.11	3.45	0.33	-2.4	2.5	0.01	348.68	16.6
Art	5.3	100	4.3	3.39	4.01	0.42	5.4	7.2	23	16.7	5.46	0.13	0.91	5.58	-7.6	1.15	0.01	69.64	2.12
CG4	5.8	212	16.7	9.29	8.35	1.46	4.5	7.5	113	<5	7.14	0.24	1.22	6.71	-5.7				
PIP	5.4	257	15.9	9.32	4.97	0.84	3.1	10.04	137	<5	22.06	0.38	2.35	0.76	-3.8				
PIF	5.8	312	30.4	10.16	20.46	6.48	3.6	11.25	169	11.8	4.04	0.16	1.27	2.46	-4.9	1.85	0.02	45.19	1.65
IHF	6.5	168	15	3.76	12.04	0.83	5.3	16.58	63	17	0.26	0.53	0.14	8.11	-15.7	1.87	0.01	4.05	0.16
FH	6.5	169	21.2	2.69	7.67	1	4.1	14	64	16.1	0.098	0.43	0.01	9.57	-15.2	1.73	0.01	1.66	0.07
AuE	5.8	52	3.8	1.98	2.27	0.2	3.1	7.05	12	7.8	2.07	0.05	0.09	2.52	-22.6	1.65	0.01	2.66	0.12
F9	5.8	38	3.3	0.78	2.46	0.26	3.2	7.13	8	<5	0.85	0.02	0.02	4.06	-27.0				
Sop	6.4	92	8.4	2.05	6.26	0.49	5.2	13.57	32	5.7	<0.005	0.005	0.12	6.13	-18.3	1.06	0.02	4.79	0.24
Mey	6	64	4.3	1.8	2.68	0.28	3.6	6.77	19	7.8	2.29	0.05	5.72		-17.6				
PIG	5.7	809	42.7	35.47	71.52	4.75	58.2	54.56	>204	12.8	17.35	1.81	2.64	0.56	-4.5				
Ton	5.1	195	11.9	7.24	6.57	0.79	10.7	16.73	71	<5	13.33	0.92	2.24	0.84	-3.9				
Bar	5.3	239	12.1	9.77	17.36	1.16	5.6	27.22	114	<5	9.95	1.2	2.10	0.77	-4.2	1.1	0.02	106.93	3.12
Ger	5.7	185	15.3	7.55	9.74	1.23	5.9	11.61	92	<5	4.15	0.19	1.28	3.63	-5.9				
Sau	5.5	336	27.9	13.38	12.26	1.33	5.5	10.04	182	<5	31.95	0.7	2.14	2.3	-3.9				
Del	5.6	298	22.7	14.15	16.03	2.12	3.5	10.94	170	<5	6.54	0.17	1.39	3.61	-4.7	0.92	0.01	278.02	11.42
TdB	5.9	856	108.8	46.28	20.12	1.8	4.4	20.12	539	<5	51.91	2.76	3.12	0.27	-2.1				
Vic	5.2	287	19.5	13.76	7.84	1.19	3.8	23.36	131	<5	37.52	2.72	2.08	1.26	-2.9				
Ern	5.8	863	46.6	30.3	104.49	5.09	59.6	9.77	414	<5	8.34	0.76	2.32	1.82	-2.9				
Bein	5.4	167	10.3	6.24	3.21	0.52	5.8	8.13	66	<5	13.14	0.47	1.3	3.92	-4.0				
PdI	6.3	2440	418.6	<0.4	68.71	5.78	37.8	12.61	1736	14.6	29.3	6.26	2.89	1.03	-1.8				
BerI	6.3	323	28.2	8.56	7.16	1.2	14.2	8.8	165	5.2	25.49	2.1	0.95	5.49	-3.4				
Har	5.8	672	38.4	37.2	45.02	2.88	26.6	33.3	366	<5	14.86	0.73	2.49	2.54	-2.9				
VQ	CGE	Spring													-2.1	4.4		1880	
SQ	CGE	Spring													-2.0	4.5		1520	
LaS	Gaz	Mofette														5.4		38	
W10	CGE	Well														5.6		1380	
MORB																8.1		1000	
Tap																0.971	0.052	0.292	0.013

**Table 1.** Analysis results for the 30 samples. CGB = Carbogazeous water from Bru area; CGS = carbogazeous water from Spa area, NCGB= non-carbogazeous water from Bru area, NCGS = non-carbogazeous water from Spa area, CGM = carbogazeous water from Malmedy area. R/Ra is the He isotopic ratio expressed with regards to ration in air. VPDB is the Viennea PeeDee Belemnite standard reporting the abundance of carbon. DIC stands for dissolved inorganic carbon.

All the data obtained from these groundwater samples of Spa, Bru and Malmedy (cations, anions, dissolved CO<sub>2</sub>, <sup>3</sup>He/<sup>4</sup>He and <sup>4</sup>He/<sup>20</sup>Ne ratios) are available in Table 1.

## 5 Discussion

### 5.1 Chemical composition of groundwater and dissolved gases

120 The Piper diagram presented in Figure 4 shows the relative proportion of cations and anions for each sample. The Figure shows a calcium magnesium bicarbonate type for most samples. Regarding the cations (Ca, Mg, Na+K), the majority of the samples have rather closed compositions and display globally balanced composition, the less abundant cation representing in any case at least 10 per cent of the total. CGB samples compensate a smaller proportion of Na+K with a bigger proportion of Mg, compared to CGS samples. One exception to this balanced composition in cations, is the *Pdl* sample, which is computed on  
125 a near-pure calcium pole, probably because it was sampled ~~located~~ in a zone influenced by the carbonate-rich conglomerate of the Graben of Malmedy (shown in Figure 3). The distinction between CG and NCG groundwater samples is much clearer looking at their anions compositions. There is a significant relative enrichment of CG samples in bicarbonates, due to the presence of dissolved CO<sub>2</sub>. Only the samples *Art* and *PIG* range out of this carbonate-rich cluster. However this lower carbonate content is only relative as the sample *Art* has a much higher concentration in sulfates (16.7 mg/l whereas most samples are <5  
130 mg/l), presumably from a local geological origin, and the sample *PIG* has a higher chloride content (58.2 mg/l, whereas the average composition of the other samples is around 5 mg/l). The latter is presumably from anthropic origin.

This figure indicates that both CO<sub>2</sub>-rich and non CO<sub>2</sub>-rich groundwaters have initially similar compositions, mainly driven by the local lithologies. The enrichment of CO<sub>2</sub> and bicarbonates in groundwater leads to an acidification of groundwater.  
135 Hence, CO<sub>2</sub>-rich groundwaters are generally more aggressive and more mineralized. However, the waters of this dataset keep the same relative proportions in cations composition, whatever their carbonate contents (Figure 4). This observation is not really in line with the hypothesis that carbonate dissolution explains the main origin of this dissolved CO<sub>2</sub>. As discussed in Barros et al. 2021, this hypothesis was until now the most commonly accepted for the CO<sub>2</sub> origin. Indeed, if the presence of dissolved CO<sub>2</sub> in carbogaseous waters was due to carbonate dissolution, it would be expected that this groundwater would have  
140 also be enriched in Ca<sup>2+</sup> and possibly Mg<sup>2+</sup> ions, in comparison to non-carbogaseous waters, but this is not the case in these Spa-Bru waters.

### 5.2 Constraining gas origin with helium and carbon isotopes

Inorganic carbon isotopes have proven to be a very powerful tool to make the distinction between different carbon sources.  
145 This isotopic proxy is particularly adapted to sparkling mineral waters (Fillimonova et al. 2020; Carreira et al. 2014; Redondo and Yelamos 2004). However, the contribution of each carbon source is sometimes difficult to deconvolve. For example, a bulk



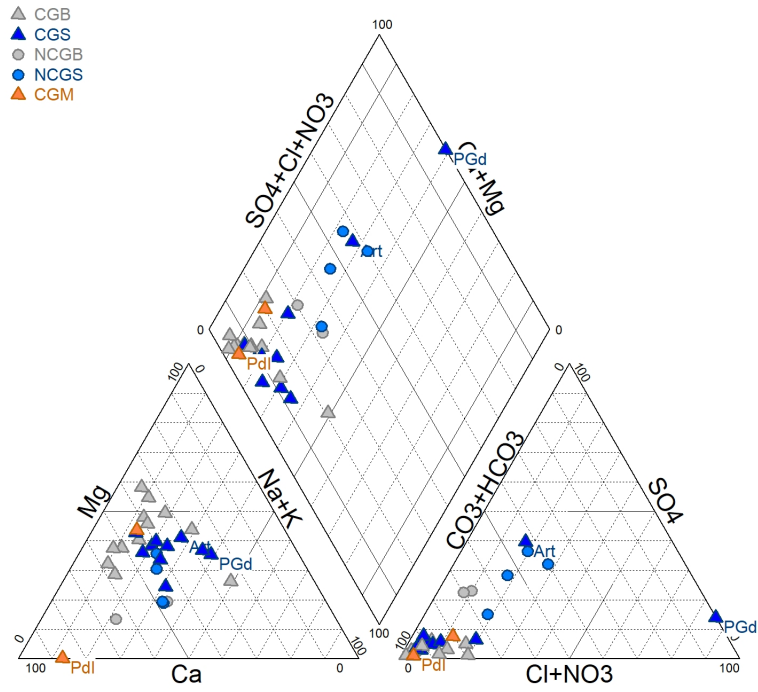


**Figure 4.** Piper diagram representing the relative proportion of cations and anions for each sample. CGB = carbogazeous water from Bru area; CGS = carbogazeous water from Spa area, NCGB= non-carbogazeous water from Bru area, NCGS = non-carbogazeous water from Spa area, CGM = carbogazeous water from Mamedy area.

C composition resulting from the mixing between marine limestones ( $\delta^{13}C \approx 0 \text{‰}$ ) and organic sediments ( $\delta^{13}C \approx -20\text{‰}$ ) may have a  $\delta^{13}C$  similar to that of mid-oceanic ridge basalts (MORB) ( $\delta^{13}C \approx -6.5 \pm 2.5 \text{‰}$ ), as shown by Sano and Marty (1995). Atmospheric  $\delta^{13}C$  is estimated around  $-8 \text{‰}$  (Karolyte et al. 2019).

150

The  $\delta^{13}C$  of inorganic carbon measured in our samples range between  $-8.8 \text{‰VPDB}$  and  $-1.8 \text{‰VPDB}$  for CG groundwater samples and between  $-27 \text{‰VPDB}$  and  $-15.2 \text{‰VPDB}$  for NCG groundwater samples. The distinction between CG and NCG groundwaters is clear: NCG groundwaters have much lighter carbon isotopic ratios. The majority of  $\delta^{13}C$  values in  $\text{CO}_2$ -rich groundwater are clustered around the mantle endmember, but some of them may also be compatible with a limestone origin (Figure 5).

155

The combination of  $\delta^{13}C$  with the  $\text{CO}_2/{}^3\text{He}$  ratio permits to make the distinction between the three main sources of dissolved carbon (mantle, limestone, organic carbon; Sano and Marty, 1995), as shown in Figure 5: the production of  ${}^3\text{He}$  in the crust being negligible (Andrews and Kay 1982), a high  ${}^3\text{He}$  content (and hence a low  $\text{CO}_2/{}^3\text{He}$  ratio) is the signature of a mantle carbon input. It can be observed in Figure 5 that  $\text{CO}_2$ -rich groundwater samples have  $\text{CO}_2/{}^3\text{He}$  and  $\delta^{13}C$  that are compatible with, (or very close to), the mantle MORB endmember. These compositions are quite close to those of the volcanic gas of the Eifel area (Marty et al., 2020) (*SQ*, *VQ* samples). Although the Spa-Bru CG groundwaters have  $\delta^{13}C$  values quite close to a limestone source, their  $\text{CO}_2/{}^3\text{He}$  is 2 to 4 orders of magnitude lower than the limestone endmember. Their clear enrichment in  ${}^3\text{He}$  demonstrates that the gas dissolved in the Spa-Bru groundwaters has a mantellic origin, probably from the nearby Eifel volcanic field.

165

Although most of the CG waters are close to the mantle endmember in this  $\text{CO}_2/{}^3\text{He}$  vs  $\delta^{13}C$ , some data points do not perfectly match the mixing lines between the three endmembers. Other processes that may have fractionated the initial  $\text{CO}_2/{}^3\text{He}$  and  $\delta^{13}C$  signatures thus need to be considered (e.g. Ray 2009, Barry et al. 2020).  $\text{CO}_2$  and helium having different solubilities, partial degassing may fractionate the  $\text{CO}_2/{}^3\text{He}$  ratio. However, the solubility of  $\text{CO}_2$  being larger than the one of helium, this process should lead to increase the  $\text{CO}_2/{}^3\text{He}$  of waters affected by degassing ratio, contrary to what we observe here. Moreover, there is almost no correlation between the  $\text{CO}_2/{}^3\text{He}$  ratios and the dissolved helium concentrations (after correction for atmospheric helium), an observation that makes this process unlikely (Table 1). Another physical process that has the ability to modify the initial  $\text{CO}_2/{}^3\text{He}$ - $\delta^{13}C$  signature is the precipitation of calcite, leading to lower the  $\delta^{13}C$  and the  $\text{CO}_2/{}^3\text{He}$  by a Rayleigh distillation (in open system). In Figure 5, following (Ray 2009, Barry et al. 2020)), we modeled the effect of calcite precipitation at various temperatures ( $50^\circ\text{C}$ ,  $100^\circ\text{C}$  and  $150^\circ\text{C}$ ), assuming an initial gas composition similar to the Eifel endmember Marty2020). Although this process may, in theory, explain part of the scatter observed within the carbogaseous sources of Spa and Bru, we should however be cautious because calcite precipitation has never been observed in any of the many boreholes that have been installed in the area for water production, in the underlying rocks where these fluids are supposed to have transited. It is nevertheless important to stress that this fractionation does not hamper the identification of a clear mantle signature.

180

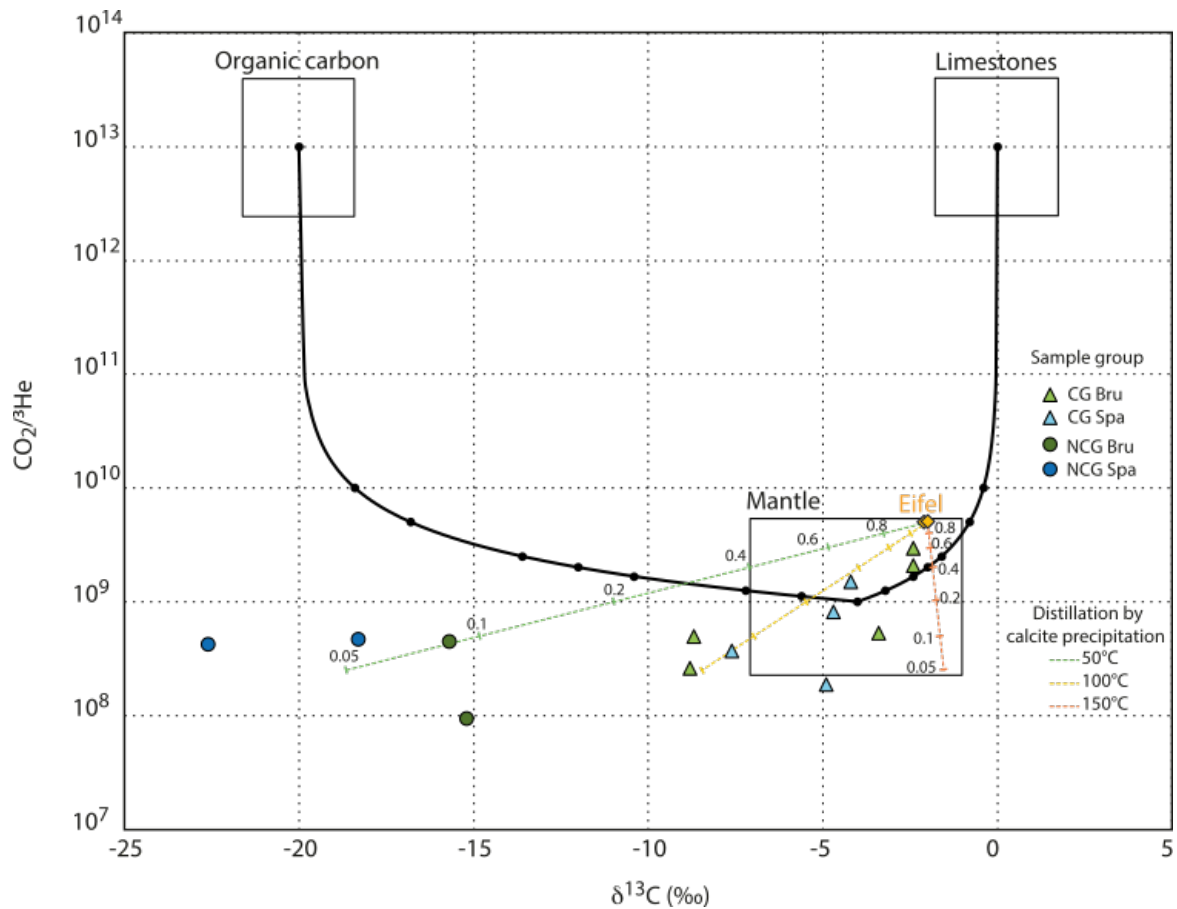


**Figure 5.**  $\text{CO}_2/{}^3\text{He}$  ratios vs  $\delta^{13}\text{C}$  values for groundwater samples in relation to mixing between the mantle, carbonate and organic  $\text{CO}_2$  endmembers based on Sano and Marty (1995) (Sano and Marty 1995). CGB = Carbogazeous water from Bru area; CGS = carbogazeous water from Spa area, CGE = Carbogazeous water from Eifel area; NCGB = non-carbogazeous water from Bru area, NCGS = non-carbogazeous water from Spa area. Gas Eifel composition from (Marty et al., 2020).  $VQ$ ,  $SQ$  and MORB are depicted from the values presented in Marty et al. (2020) (Marty et al. 2020). All  $\text{CO}_2$ -rich groundwater samples fall in or close to the mantle range. Non- $\text{CO}_2$ -rich groundwater samples present much lighter C isotopic composition. The impact of calcite precipitation at three temperature (50, 100 and 150°C) is modeled assuming an open system Rayleigh distillation, following (Ray et al., 2009) and (Barry et al., 2020)

The low  $\delta^{13}\text{C}$  and  $\text{CO}_2/{}^3\text{He}$  values of the noncarbogazeous sources stand below the pure mixing curve between the mantle and organic carbon endmembers (Figure 5). Our geochemical dataset (Table 1) shows that these gas poor fluids are noncarbogazeous groundwaters, that have never been enriched with gaz, explaining their very different composition and depletion of  $\delta^{13}\text{C}$  and  $\text{CO}_2$ .

### 5.3 Discriminating He origin with He and Ne isotopes

He isotopic ratios are normalized against the atmospheric isotopic composition and are expressed in  $R_a$  (considering atmospheric  ${}^3\text{He}/{}^4\text{He} = R_a = 1.382 \times 10^{-6}$  (Sano and Fischer 2013)). In these waters,  $R_a$  range between 0.92 and 2.70 ( $\pm 0.02$ ).  ${}^4\text{He}/{}^{20}\text{Ne}$  ratios are very variable with values ranging from 1.7 to 348.7 ( $\pm 4\%$ ). Based on the measured  ${}^4\text{He}/{}^{20}\text{Ne}$  ratios, and assuming all  ${}^{20}\text{Ne}$  of atmospheric origin, the contribution of atmospheric He can be computed using mixing equation 1, where  ${}^4\text{He}/{}^{20}\text{Ne}_{air}$  is considered equal to 0.267 according to (Holocher et al. 2001) and  ${}^4\text{He}/{}^{20}\text{Ne}_{mantle}$  is equal to 1000 according to Dunai and Baur 1995.

$$\%He_{atm} = \frac{1 - \frac{{}^4\text{He}/{}^{20}\text{Ne}_{mantle}}{{}^4\text{He}/{}^{20}\text{Ne}_{sample}}}{1 - \frac{{}^4\text{He}/{}^{20}\text{Ne}_{mantle}}{{}^4\text{He}/{}^{20}\text{Ne}_{air}}} \quad (1)$$

This shows that atmospheric helium is negligible for all CG samples (less than 0.5 %) but more important for NCG samples (between 5 and 15 %). The measured  ${}^3\text{He}/{}^4\text{He}$  ratios allow the computation of the origin of helium, which appears to be a mixture of crustal and mantle helium. The proportion of each source (crust and mantle) may be computed according to mixing equations 2 and 3, where  ${}^3\text{He}/{}^4\text{He}_{crust}$  and  ${}^3\text{He}/{}^4\text{He}_{mantle}$  are taken equal to 0.02 and 6.5 Ra, respectively according to Dunai and Baur (1995). We chose this 6.5 Ra "mantle" endmember as representative of the subcontinental lithospheric mantle (Dunai and Baur, 1995).

$$\%He_{mantle} = \frac{(1 - \%He_{atm})({}^3\text{He}/{}^4\text{He}_{crust} - {}^3\text{He}/{}^4\text{He}_{sample})}{{}^3\text{He}/{}^4\text{He}_{crust} - {}^3\text{He}/{}^4\text{He}_{mantle}} \quad (2)$$

$$\%He_{crust} = 1 - \%He_{mantle} \quad (3)$$

Crust-mantle mixing lines are also displayed in Figure 6.

Helium present in groundwater samples appears to be between 50 and 80 % from crustal origin. A distinction can be made between CG samples from Spa and Bru area, samples from Spa displaying more crustal helium (from 66 to 81%) than those of Bru (ranging from 54 to 57%). This may result from the local lithologies: Cambrian and Ordovician rocks from the Stavelot Massif are known for their high uranium content, often leading to high radon concentrations in cellars and underground buildings and also  ${}^4\text{He}$  production through alpha-decay (Depret et al. 2021; H.W. 2011). CG samples of Spa also differ from Eifel samples since they bear a larger proportion of crustal helium than the groundwaters of this volcanic region, where more than 80% of He is from the mantle.

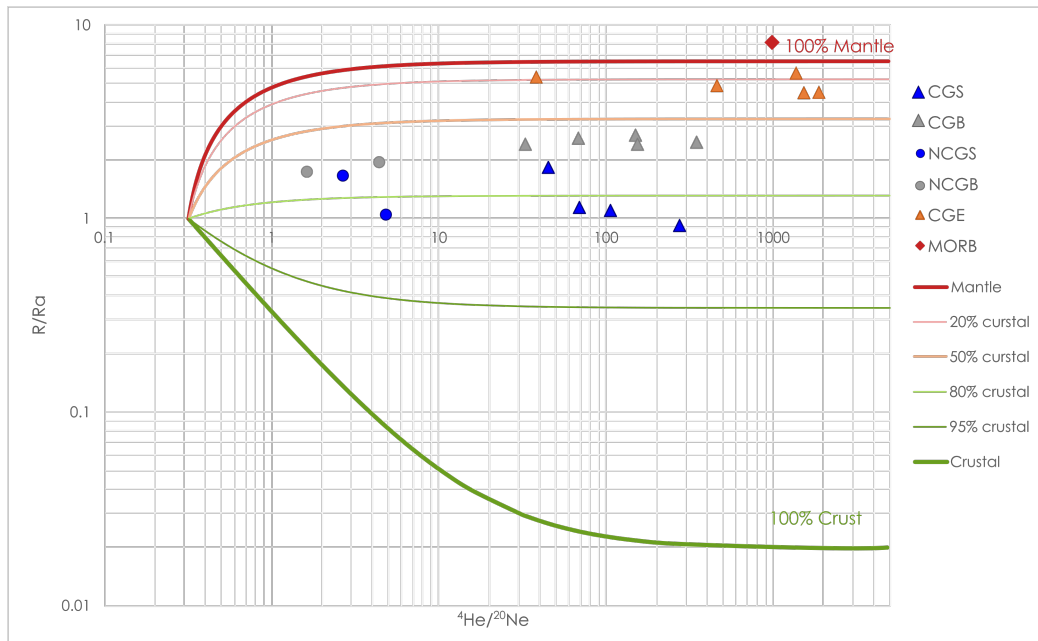


**Figure 6.** Proportion of crustal and mantle He in the samples, based on  $R/Ra$  and  ${}^4He/{}^{20}Ne$  values. CGB = Carbogazeous water from Bru area; CGS = carbogazeous water from Spa area, CGE = Carbogazeous water from Eifel area; NCGB = non-carbogazeous water from Bru area, NCGS = non-carbogazeous water from Spa area. Mixing lines are computed from Equations 3 and 2. Values from Eifel and MORB are depicted from Marty et al. (2020) (Marty et al. 2020). He atmospheric contribution is negligible. He crustal contribution appears to be more important for CG samples from the Spa area, as the local lithology is richer in uranium minerals.

#### 5.4 Conceptual model of groundwater and gaz circulation

215  $CO_2/{}^3He$  and  $\delta^{13}C$  measured in the samples from Eastern Belgium springs show that the dissolved  $CO_2$  present in the springs  
 from east Belgium originates from a mantle contribution. The similar cation proportions for both CG and NCG groundwaters  
 support the hypothesis that both groundwater types are initially the same (i.e., having the same origin). This is at odds with the  
 commonly accepted hypothesis according to which CG groundwater would travel at several kilometers in-depth to meet and  
 dissolve carbonated layers, where it could have acquired its dissolved  $CO_2$  content before upflowing rapidly to the surface.  
 220 This hypothesis is also whittled by the fact that CG groundwaters are cold groundwaters, having similar temperatures to NCG  
 groundwaters, between 12 and 13°C. Assuming a vertical temperature gradient of 30°C/km, this suggests that water circulation  
 does not occur deeper than a few hundred of meters below the surface.  ${}^3He/{}^4He$  ratios indicate that crustal  ${}^4He$  enrichment  
 occurred during the water circulation in the aquifer, but such addition of crustal fluid is impossible in less than 1 km flow water  
 paths.

225

The conceptual circulation model of water and gas at depth has then to be updated and is shown in Figure 7. The conceptual model was very similar to one of the models described by Pisolkar (2017) in his work aiming at developing integrated hydro-geological models representing the classical properties of CO<sub>2</sub>-rich mineral waters systems in different contexts.

230 Considering all our data with those of Barros et al. (2021) (notably the isotopic  $\delta^{18}O$  and D/H composition of the water), we propose here a revised model (Figure 7) to explain the origin of the gas-rich groundwaters of the Spa-Bru massif, involving the input of CO<sub>2</sub>-<sup>3</sup>He rich gas from the nearby Eifel massif through deep crustal faults.

The geomorphology of the system is mostly controlled by basin structures and anticlines. Slate beds act as low permeability barriers partitioning the aquifer and isolating the different compartments. Small faults and surface weathering enable the infiltration and storage of water from the surface to the underground, whereas major deep-rooted faults act as CO<sub>2</sub> transport pathway from degassing mantle that can be located several tens of km away to the local aquifers. Where major faults reaching the surface do not encounter a sufficiently permeable and water-saturated zone (i.e. in the slates covered by a clayey colluvium as a result of weathering processes), CO<sub>2</sub>-<sup>3</sup>He rich dry gas are discharged to the surface and mofette are observed. The discharge points are mainly springs (at low topographic points or at geological low permeability/high permeability contacts) in the hillslopes or water abstraction wells.

The CO<sub>2</sub>/<sup>3</sup>He and  $\delta^{13}C$  composition of the samples is very close to samples taken in the Eifel Volcanic Fields (Figure 5, Table 1) and considering the proximity of the two sites (distance lower than 100 km), it seems very likely that the gas found in the Belgian springs comes from the degassing of the mantle in the Eifel Volcanic Fields. In the future, the link between the two regions needs to be further explained in terms of structural geology.

The main structural feature existing in the area are the Eupen thrust fault, the Xhoris thrust fault, and the normal faults linked to the opening of the Malmedy Graben (see Figure 1). All these faults could be connected at several kilometers in-depth to the Midi-Eifel thrust fault, a major thrust fault corresponding to the northernmost front of the Variscian Orogeny and connecting both regions. This fault acts as an important seismic reflector and could thus be observed below the Stavelot Massif thanks to seismic measurements surveys lead by the DEKORP research group in the early nineties (Stiller et al. 1987).

The exact origin of the Eifel Volcanism, between a plume or an upper-mantle contribution, is still a matter of debate. Unfortunately, although the results confirm the magmatic origin of the gas dissolved in groundwater, they do not provide new information to support one or the other hypothesis.

## 6 Conclusions and future research

This paper answers a long-standing question regarding the origin of the dissolved CO<sub>2</sub> in the naturally sparkling mineral waters of eastern Belgium. The combination of  $\delta^{13}C$  and <sup>3</sup>He isotopes have shown with a high level of confidence that the dissolved

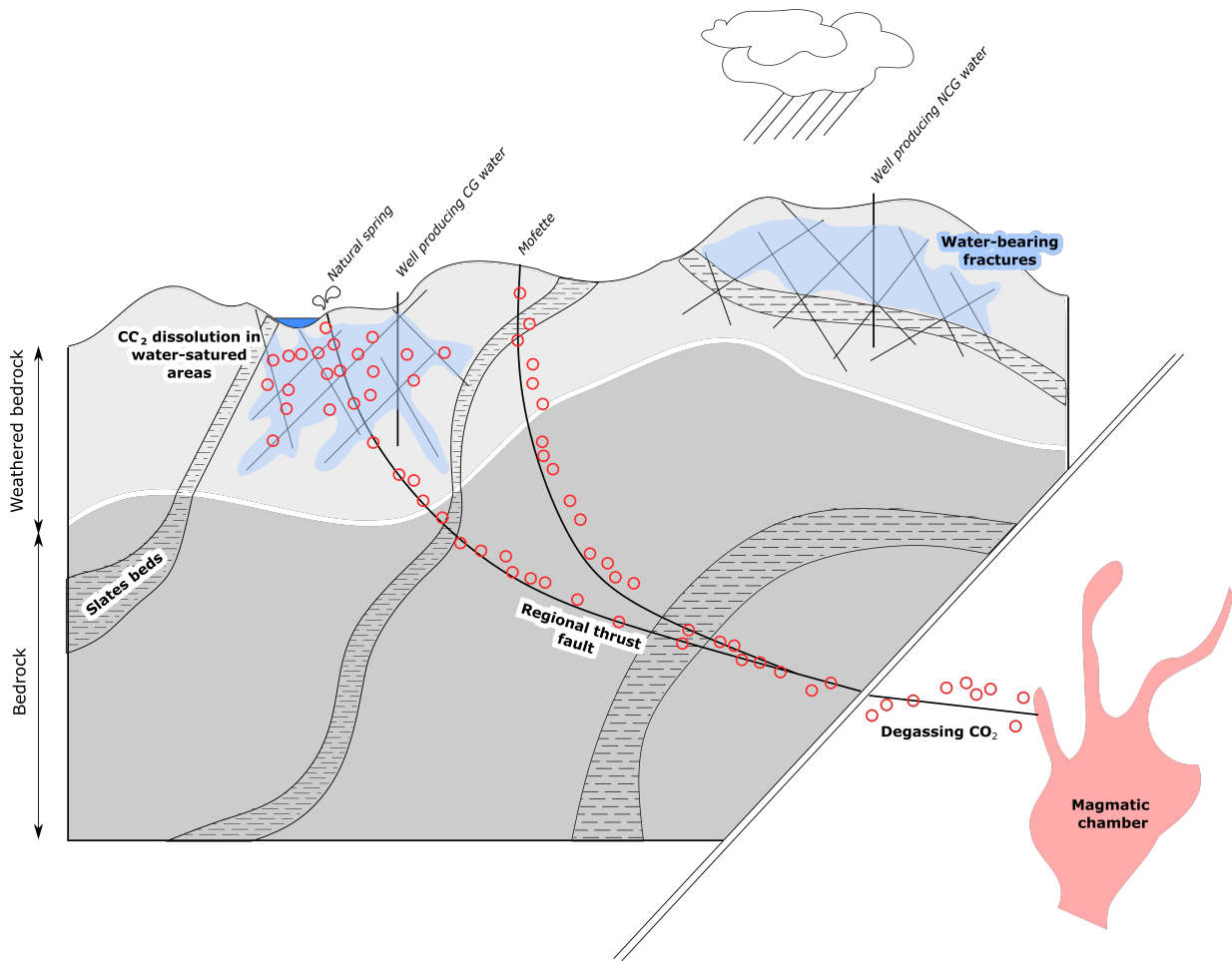


**Figure 7.** Updated conceptual model for the existence of CG and NCG groundwaters. Aquifer zones are located in the weathered parts of the bedrocks. The aquifer in fractured and slates beds isolate aquifers zones one from the other. Degassing CO<sub>2</sub> from the mantle is brought to the system through regional thrust faults, and dissolved in groundwater.

CO<sub>2</sub> in groundwater from the springs and in boreholes was from mantle origin, and can be very likely attributed to the degassing  
260 of the mantle in the neighboring Eifel volcanic Fields, located at a distance lower than 100 km eastward. The role of the deep-  
rooted fractures that act as CO<sub>2</sub> transport pathway to the surface are still to be clarified, but several major thrust faults exist in  
the Rhenish Massif and could have connected the Eifel area with the studied area.

*Author contributions.* Agathe Defourny : Conceptualization, Methodology, Investigation, Writing – Original Draft, Visualization Pierre-  
Henri Blard : Validation, Resources, Funding Acquisition, Writing – Review Editing Laurent Zimmermann : Validation, Resources, Data  
265 Curation Patrick Jobé : Supervision Arnaud Collignon: Supervision, Resources Frédéric Nguyen : Supervision Alain Dassargues : Supervi-  
sion, Project administration, Funding acquisition, Writing – Review Editing

*Competing interests.* No competing interests are present in this manuscript.

*Acknowledgements.* This work is part of the ROSEAU project, as part of the Walloon program "Doctorat en Entreprise", co-funded by the  
SPW Région Wallonne of Belgium and the company Bru-Chevron S.A. (Spadel S.A.), under grant number 7984. The collaboration with the  
270 CRPG of Nancy was made possible thanks to the Europlanet Transnational Access Program, as this project has received funding from the  
European Union's Horizon 2020 research and innovation program under grant agreement No 871149. The authors acknowledge these two  
institutions for their support.



## References

- [Aes+96] W. Aeschbach-Hertig et al. “Quantification of gas fluxes from subcontinental mantle: the example of Laacher See, a maar lake in  
275 Germany”. In: *Geochimica et Cosmochimica Acta* 60 (1996), pp. 31–41. URL: [https://doi.org/10.1016/0016-7037\(95\)00370-3](https://doi.org/10.1016/0016-7037(95)00370-3).
- [Agn18] Robert J. Agnew. “Why springs bubble: A framework for gas discharge in groundwater”. In: *Groundwater* 56.6 (2018), pp. 859–  
870. URL: <https://doi.org/10.1111/gwat.12789>.
- [AK82] J. Andrews and R. Kay. “Natural production of tritium in permable rocks”. In: *Nature* 298 (1982), pp. 361–363. URL: <https://doi.org/10.1038/298361a0>.
- 280 [Bar+21] R. Barros et al. “A review of the geology and origin of CO<sub>2</sub> in mineral water springs in east Belgium”. In: *Geologica Belgica*  
24.1-2 (2021). URL: <https://doi.org/10.20341/gb.2020.023>.
- [Bar+20] Peter H. Barry et al. “Volatile sources, sinks and pathways: A helium-carbon isotope study of Baja California fluids and gases”.  
In: *Chemical Geology* 550 (2020), p. 119722. ISSN: 0009-2541. URL: <https://www.sciencedirect.com/science/article/pii/S0009254120302618>.
- 285 [Bek+19] D.V. Bekaert et al. “Novel insights into the degassing history of the Earth’s mantle from high precision noble gas analysis of  
magmatic gas”. In: *Earth and Planetary Science Letters* 525 (2019), p. 115766. URL: <https://doi.org/10.1016/j.epsl.2019.115766>.
- [Brä+13] K. Bräur et al. “Indications for the existence of different magmatic reservoirs beneath the Eifel area (Germany): A multi-isotope  
(C,N,He,Ne,Ar) approach”. In: *Chemical Geology* 56.3 (2013), pp. 193–208. URL: <https://doi.org/10.1016/j.chemgeo.2013.08.013>.  
290
- [Car+14] P.M. Carreira et al. “Carbon isotopes and geochemical processes in co<sub>2</sub>-rich cold mineral water, N<sub>P</sub>ortugal”. In: *Environmental  
Earth Sciences* 71 (2014), pp. 2941–2953.
- [Dep+21] M. Depret et al. “Mineralogical and hydrogeological study of "pouhons" in the lower Paleozoic formations of the Stavelot-Venn  
Massif”. In: *Geologica Belgica* in press (2021). URL: <https://doi.org/10.20341/gb.2021.001>.
- 295 [DB95] T. Dunai and H. Baur. “Helium, neon, and argon systematics of the European subcontinental mantle: Implications for its geo-  
chemical evolution”. In: *Geochimica et Cosmochimica Acta* 59 (1995), pp. 2767–2783. URL: [https://doi.org/10.1016/0016-7037\(95\)00172-V](https://doi.org/10.1016/0016-7037(95)00172-V).
- [FM99] W. Fielitz and J.-L. Mansy. “Pre- and synorogenic burial metamorphism in the Ardenne and neighbouring areas (Rhenohercynian  
zone, central European Variscides”. In: *Tectonophysics* 309.1-4 (1999), pp. 227–256. URL: [https://doi.org/10.1016/S0040-1951\(99\)00141-9](https://doi.org/10.1016/S0040-1951(99)00141-9).  
300
- [Fil+20] E. Fillimonova et al. “Hydrogeology and hydrochemistry of mineral sparkling groundwater within Essentuki area (Caucasian  
mineral water region)”. In: *Environmental Earth Sciences* 79.15 (2020). URL: <https://doi.org/10.1007/s12665-019-8721-2>.
- [Gil+19] S.M.V. Gilfillan et al. “Noble gases confirm plume-related mantle degassing beneath Southern Africa”. In: *Nature Communica-  
tions* 10:5028 (2019). URL: <https://doi.org/10.1038/s41467-019-12944-6>.
- 305 [GSB99] S. Goes, W. Spakman, and H. Bijwaard. “A lower mantle source for central European volcanism”. In: *Science* 286 (1999),  
pp. 1928–1931.

- [HW11] Vanderschueren H.W. “Le radon dans l’air, dans l’eau et dans les roches. Mesure dynamique de son exhalation et contribution á la caractérisation géologique des matériaux.” In: *Geological survey of Belgium professional paper* 308 (2011), 96p.
- [Hol+01] J. Holocher et al. “Noble gas and major element constraints on the water dynamics in an alpine floodplain”. In: *Groundwater* 39 (2001), pp. 841–852.
- [Kar+19] R. Karolyte et al. “Tracing the migration of mantle CO<sub>2</sub> in gas fields and mineral water springs in south-east Australia using noble gas and stable isotopes”. In: *Geochimica et Cosmochimica Acta* 259 (2019), pp. 109–128. URL: <https://doi.org/10.1016/J.gca.2019.06.002>.
- [KBD20] C. Kreemer, G. Blewitt, and P. M. Davis. “Geodetic evidence for a buoyant mantle plume beneath the Eifel volcanic area, NW Europe”. In: *Geophysical Journal International* 222 (2020), pp. 1316–1322. URL: <https://doi.org/10.1093/gji/ggaa227>.
- [Mar+20] B. Marty et al. “An evaluation of the C/N ratio of the mantle from natural CO<sub>2</sub>-rich gas analysis : Geochemical and cosmochemical implications”. In: *Earth and Planetary Science Letters* 551 (2020), p. 116574. URL: <https://doi.org/10.1016/J.epsl.2020.116574>.
- [MHN96] F. May, S. Hoernes, and H.J. Neugebauer. “Genesis and distribution of mineral waters as a consequence of recent lithospheric dynamics: the Rhenish Massif, Central Europe”. In: *Geologische Rundschau* 85 (1996), pp. 782–799. URL: <https://doi.org/10.1007/s005310050112>.
- [Mor+18] M. Moreira et al. “The xenon isotopic signature of the mantle beneath Massif Central”. In: *Geochimica et Cosmochimica Acta* 192 (2018), pp. 28–32.
- [Ray09] Jyotiranjana S. Ray. “Carbon isotopic variations in fluid-deposited graphite: evidence for multicomponent Rayleigh isotopic fractionation”. In: *International Geology Review* 51.1 (2009), pp. 45–57. DOI: 10.1080/00206810802625057. URL: <https://doi.org/10.1080/00206810802625057>.
- [RY04] R. Redondo and J. G. Yelamos. “Determination of CO<sub>2</sub> origin (natural or industrial) in sparkling bottled waters by <sup>13</sup>C/<sup>12</sup>C isotope ratio analysis”. In: *Food Chemistry* 92 (2004), pp. 507–514.
- [Rit+01] J.R.R. Ritter et al. “A mantle plume below the Eifel volcanic fields, Germany”. In: *Earth and Planetary Science Letters* 186 (2001), pp. 7–14. URL: [https://doi.org/10.1016/S0012-821X\(01\)00226-6](https://doi.org/10.1016/S0012-821X(01)00226-6).
- [SF13] Y. Sano and T.P. Fischer. “The analysis and interpretation of noble gases in modern hydrothermal systems”. In: *The Noble Gases as Geochemical Tracers*. Ed. by P. Burnard. Springer, 2013, pp. 249–317.
- [SM95] Y. Sano and B. Marty. “Origin of carbon in fumarolic gas from island arcs”. In: *Chemical Geology* 119 (1995), pp. 265–274.
- [Sti+87] M. Stiller et al. *Deep seismic reflection profile DEKORP 1987-1A across the western Rhenish Massif, West Germany/ East Belgium*. 1987. URL: <https://doi.org/10.5880/GFZ.DEKORP-1A.001>.
- [VBJ02] Y. Vanbrabant, J. Braun, and D. Jongmans. “Models of passive margin inversion: implications for the Rhenohercynian fold-and-thrust belt, Belgium and Germany”. In: *Earth and Planetary Science Letters* 202 (2002), pp. 15–29. URL: [https://doi.org/10.1016/S0012-821X\(02\)00751-3](https://doi.org/10.1016/S0012-821X(02)00751-3).